

RESEARCH

Open Access



Hierarchical network modulation of cell death regulators and inflammatory genes by biogenically engineered gold nanoconstructs with CK in gastric tumorigenesis

Abdus Samad¹, Abishek Gnanasekaran¹ and Yeon Ju Kim^{1*}

*Correspondence:
yeonjukim@khu.ac.kr

¹ Graduate School of Biotechnology, College of Life Science, Kyung Hee University, Yongin-Si 17104, Republic of Korea

Abstract

Background: Gastric cancer (GC) progression is influenced through the dysregulation of the cell death and chronic inflammation, which together foster a tumor-promoting microenvironment and enhance cancer cell survival. Targeting these pathways could provide novel therapeutic strategies. In a previous study, we synthesized gold nanoparticles (GNPs) using *Bifidobacterium animalis* subsp. *lactis* (BAL) and compound K (CK), leading to the creation of BAL-CK-GNPs. This study aims to investigate the anti-gastric cancer potential of BAL-CK-GNPs against three cancer cell lines, including A549, HT-29, and AGS cells.

Results: Our findings demonstrated that BAL-CK-GNPs exerted the highest inhibitory effect ($IC_{50} = 43.72 \mu\text{g/mL}$) on AGS cells. We confirmed their cellular uptake and penetration using enhanced dark field microscopy and assessed apoptosis induction through Hoechst and PI staining. Apoptotic effects were further supported by mitochondrial disruption, visualized with Mito-tracker staining, and transmission electron microscopy, which revealed the cellular localization of BAL-CK-GNPs. Therefore, gene expression analysis revealed the upregulation of apoptotic markers, supporting apoptosis induction. Subsequent transcriptomics analysis identified significant changes in differentially expressed genes (DEGs), with BAL-CK-GNPs treatment suppressing 78 and stimulating 146. Notably, these included glutathione metabolism pathways, as well as cell death pathways (ferroptosis and necroptosis) and inflammatory pathways (NF- κ B, IL-17, TNF, chemokines, and cytokines). Among these DEGs, eight key regulators (IFI35, DDX58, IFIT1, ISG15, EIF2AK2, IFIH1, FLT3LG, and IRF7) associated with cell death and inflammation were prominently affected, suggesting their roles in mediating the therapeutic effects of BAL-CK-GNPs.

Conclusions: Our findings suggest that BAL-CK-GNPs represent a promising therapeutic strategy for GC, capable of inducing apoptosis, ferroptosis, necroptosis, and modulating inflammation to inhibit GC cell growth.

Keywords: Biogenic nano-construct, Cell death (apoptosis/ferroptosis/necrosis), Inflammation, Gastroepithelial transcriptomic dysregulation, RNA sequencing



Introduction

Cancer is a highly complex and deadly disease that affects a large portion of the global population (Tran et al. 2022). Among the different types of cancer, gastric cancer (GC) is the fifth most common malignancy and is responsible for a substantial number of cancer-related deaths worldwide (Santos et al. 2024). Several factors, including chemical and microbial carcinogens, have been linked to the development and progression of GC (Das et al. 2020). Microbial pathogens trigger chronic inflammation and produce toxins that cause DNA damage, impair repair mechanisms, and disrupt cell signaling, ultimately contributing to cancer progression (Khan 2015). Recent studies have highlighted that *Escherichia coli* is associated with colorectal cancer, *Helicobacter pylori* with GC and gallbladder cancer, and *Chlamydia pneumoniae* with lung cancer (Khan et al. 2016, 2020; Wang et al. 2021). However, despite ongoing advancements in diagnostic methods, surgical treatments, and chemotherapy, many patients are still diagnosed at late stages, leading to a poor overall survival rate for gastric cancer (Guan et al. 2023). Moreover, chemotherapy and radiotherapy, though effective, are linked to severe side effects and resistance, highlighting the need for targeted therapies. Nanotechnology, particularly nanoparticles, has emerged as a promising approach for cancer treatment (Chehelgerdi et al. 2023).

Gold nanoparticles (GNPs) are gaining interest in cancer therapy due to their high surface area, biocompatibility, optical properties, and ease of modification. These features make them ideal for drug delivery, imaging, and therapeutic applications (Kumalasari et al. 2024). Compound K (CK), a metabolite of ginsenosides from *Panax ginseng*, shows promise in cancer therapy with anti-inflammatory, antioxidant, and anticancer properties. However, its clinical use is limited by poor water solubility and low bioavailability, affecting absorption and therapeutic effectiveness (Kim et al. 2024; Puja et al. 2022). To address these limitations, GNPs offer a promising solution. Recently, many researchers have developed GNPs as anti-cancer agents (Mary et al. 2024; Mi et al. 2022; Sakore et al. 2024). By loading CK onto GNPs, the compound's solubility and stability can be enhanced, enabling its targeted delivery to cancer cells and improving its therapeutic effects (Kim et al. 2024). Among various methods of synthesizing GNPs, biological synthesis using microorganisms such as bacteria, fungi, and algae is particularly advantageous due to its eco-friendly and cost-effective nature (Dhandapani et al. 2021). Recent studies highlight *Bifidobacterium* species for eco-friendly GNP biosynthesis, producing biocompatible nanomaterials with therapeutic potential. As a common gut bacterium, it also offers probiotic health benefits while enabling sustainable nanoparticle production (Santhosh et al. 2022). Utilizing *Bifidobacterium animalis* subsp. *lactis* (BAL) for BAL-CK-GNP development offers a novel strategy to enhance CK delivery and efficacy, especially in GC treatment.

Programmed cell death (PCD) pathways, including apoptosis, ferroptosis, and necroptosis, along with inflammation, critically influence GC progression and therapy resistance (Tong et al. 2022; Wang et al. 2024). Apoptosis is a non-inflammatory process that removes damaged or malignant cells through intrinsic (mitochondrial) or extrinsic (death receptor) pathways. These pathways are activated by internal stresses, such as DNA damage, or by external signals (Newton et al. 2024; Pistritto et al. 2016). However, GC cells frequently evade apoptosis, enabling uncontrolled proliferation and therapeutic

resistance, underscoring its targeting in treatment strategies (Lei et al. 2022; Peng et al. 2022). Non-apoptotic pathways such as ferroptosis and necroptosis offer alternative therapeutic avenues, particularly for apoptosis-resistant tumors (Tong et al. 2022). In addition, ferroptosis, an iron-dependent process driven by lipid peroxide accumulation and reactive oxygen species (ROS), disrupts cell membranes, rendering iron-rich cancer cells vulnerable (Jin et al. 2024). On the other hand, necroptosis, a regulated necrotic pathway activated when apoptosis is blocked, releases pro-inflammatory damage-associated molecular patterns (DAMPs), linking it to inflammation and tumor suppression (Gong et al. 2019; Sprooten et al. 2020). Another important factor is inflammation, which plays a critical role in cancer progression by fostering a tumor-friendly environment that promotes cell proliferation, angiogenesis, and metastasis case of GC (Wang et al. 2024). Inflammatory signaling pathways, including those mediated by pro-inflammatory cytokines, such as NF- κ B, TNE, and IL-17, help establish a tumor-promoting microenvironment (Aguilar-Cazares et al. 2019; Wessler et al. 2017). Targeting both PCD pathways and inflammatory mechanisms could thus improve therapeutic outcomes in GC (Aguilar-Cazares et al. 2019).

This study explores the molecular mechanisms underlying the anticancer effects of BAL-CK-GNPs in GC AGS cells. We focus on genes linked to cell death, including apoptosis, ferroptosis, necroptosis, and inflammation. The findings aim to clarify how BAL-CK-GNPs affect GC cell survival and death. These insights could guide the development of targeted therapeutic strategies for enhanced GC treatment efficacy.

Materials and methods

Materials

MRS (de Man, Rogosa, and Sharpe) broth and agar were purchased from BD Sciences (Seoul, Republic of Korea). A special grade of L-cysteine hydrochloride monohydrate ($C_3H_7NO_2S \cdot HCl$, 99.0%) was purchased from Samchun Chemicals (Seoul, Republic of Korea). Analytical grade hydrogen tetrachloroaurate (III) hydrate (gold salt) and hydrochloric acid (HCl, ACS reagent, 37%) were purchased from Sigma-Aldrich Chemicals (St. Louis, MO, USA). Soluble 3-(4,5-dimethyl-thiazol-2yl)-2,5-diphenyl tetrazolium bromide (MTT) was purchased from Life Technologies (Eugene, OR, USA). Sodium chloride (NaCl, $\geq 99.50\%$) and sodium hydroxide (NaOH, $\geq 98\%$) were purchased from Samchun Chemicals and Metals Co., Ltd, respectively. CK ($\geq 95\%$) was acquired from the ginseng bank at Kyung Hee University (Yongin, Republic of Korea). Fetal bovine serum (FBS) and penicillin–streptomycin were sourced from GenDEPOT (Barker, TX). All other chemicals and standards used in this study were of analytical grade and were used as received.

Synthesis and characterization of BAL-CK-GNPs

The synthesis of ginsenoside CK-loaded GNP followed our published protocol (Kim et al. 2024), cultivation of BAL was subcultured in MRS broth, collection of fresh biomasses, and synthesis of GNPs with CK. After ultrasonication and centrifugation, BAL-CK-GNPs were collected and resuspended in sterile water. In a previous study, we detailed a comprehensive procedure for preparing, synthesizing, and characterizing BAL-CK-GNPs (Kim et al. 2024). Various instrumental techniques were employed, as reported

previously, including ultraviolet–visible, high-resolution transmission electron microscopy, elemental mapping, X-ray diffraction, selected area diffraction, energy-dispersive X-ray, dynamic light scattering, photoluminescence, and Fourier-transform infrared.

Quantification of drug release and loading efficiency of CK-loaded BAL-CK-GNPs

Briefly, 1 mg of air-dried drug-loaded BAL-CK-GNPs was suspended in a DMSO–MeOH (1:4, v/v) mixture and sonicated overnight for complete drug release. The supernatant was filtered, and the released CK was quantified using a liquid chromatography–mass spectrometry (LC–MS) system, consisting of a Thermo Vanquish UHPLC coupled with a Thermo TSQ Altis triple quadrupole mass spectrometer. Chromatographic separation was performed using a 2.1 mm × 100 mm, 1.7 μm column, with 0.1% formic acid in distilled water (solvent A) and 0.1% formic acid in acetonitrile (solvent B) as the mobile phases. The injection volume for each sample was 3 μL, with UV detection at 203 nm. Drug release (I) and loading efficiency (II) were calculated using the following formulas:

$$(I) \text{ Drug release calculation : } y = ax + b$$

where y is the peak response, x is the drug concentration, a is the slope, and b is the intercept:

$$(II) \text{ Drug loading efficiency(\%)} = \left(\frac{\text{Total amount of drug released from NPs}}{\text{Yield of NPs}} \right) \times 100$$

Cell lines and culture environment

Human gastric adenocarcinoma cells (AGS; P23–30), human colon cancer cells (HT29; P5–11), and human lung cancer cells (A549; P8–19) were obtained from the Korean Cell Line Bank (Seoul, Republic of Korea). All cells were maintained and grown in RPMI-1640 with 10% FBS and 1% penicillin–streptomycin supplement. The cells incubation was conducted at 37 °C in a 5% CO₂ humidified environment, maintaining optimal culture conditions essential for cell growth and viability. After 80% confluence of cells used for the experiments.

Cell viability assessment of BAL-CK-GNPs

To test the cytotoxicity of BAL-CK-GNPs in various cancer cell lines (AGS, HT29, and A549), we used the MTT reduction assay. The cells were seeded onto 96-well plates at a density of 2×10^5 cells/mL and incubated overnight. Then, cells were treated with 20, 40, 60, and 80 μg/mL of BAL-CK-GNPs, while the control group cells were only exposed to the medium. After 24 h of treatment, cytotoxicity was assessed by adding 100 μL of MTT solution (0.5 mg/mL) to each well and incubating for 3 h at 37 °C in 5% CO₂. Subsequently, 100 μL of DMSO was added to dissolve the formazan crystals formed. The absorbance was then measured at 570 nm using a microplate reader, SpectraMax[®] ABS plus machine (San Jose, CA, USA). MTT experiments were conducted in triplicate across three independent runs ($n=3$) to ensure accuracy and consistency, with cytotoxic effects calculated relative to untreated control cells. The inhibitory concentration (IC₅₀) and data were analyzed using GraphPad Prism 8 (GraphPad Software, La Jolla, CA).

Transmission electron microscopy (TEM) analysis

AGS cell lines at density of 1×10^5 cells/mL were incubated in 60 mm culture dishes for 24 h at 37 °C with 5% CO₂. After 24 h, the cells were treated with BAL-CK-GNPs (60 µg/mL) and incubated for 3 h; the culture medium was discarded and washed three times with $1 \times$ PBS (pH 7.0). The cell pellet was fixed in 2.5% glutaraldehyde for 12 h. After fixation, the cell pellet was treated with 1% osmium tetroxide for 2 h. To pass through the dehydration process, ethanol (50–100%) was continuously reacted for 15 min per each concentration. This sample was subjected to a propylene oxide:epon (2:1) treatment for 24 h at 50 °C and for 48 h at 60 °C. For ultrafiltration, the sample was cut using an ultramicrotome, placed on the grids, stained with 3% uranyl acetate and lead citrate, and imaged using an 80 kV JEM-1010 TEM (JEOL, Tokyo, Japan).

Dark field microscopy analysis of synthesized nanoparticles in AGS cells

AGS cells were cultured on 18 mm coverslips at a density of 2×10^5 cells/mL overnight at 37 °C in a 5% CO₂ incubator, and then were treated with BAL-CK-GNPs (60 µg/mL). After 3 h, the cells were washed 3 times with PBS. The coverslip was placed on the slide glass and then sealed with nail polish. The sample was then observed through light scattering using a wavelength-dependent enhanced dark field microscopy system, which was an enhanced dark-field (EDF) illumination system (CytoViva Inc., Auburn, AL, USA) attached to an upright Olympus BX51 microscope (Olympus Optical Co., Ltd., Tokyo, Japan).

Fluorescence microscopy analysis

BAL-CK-GNPs-induced apoptosis was characterized using both Hoechst 33258 staining and PI staining kits following the manufacturer's instructions with slight modifications. To check for damaged mitochondria in apoptotic cells, the cells were stained with Mito-tracker kits following the instructions with slight modifications. The cells were washed twice with PBS and fixed with 4% paraformaldehyde for 10 min. Then, different concentrations of treated and untreated cells were stained with 10 µg/mL Hoechst 33258 staining solution, PI staining, and mitochondrial staining solution at 37 °C for 10 min. The stained cells were washed 3 times with PBS, and fluorescence imaging was captured using a Leica DMLB fluorescence microscope (Wetzlar, Germany). The fluorescence intensity was determined using ImageJ software.

qRT-PCR analysis of apoptosis-related genes

AGS cells were cultured in 60 mm dishes at a density of 2×10^5 cells/mL for 24 h, followed by treatment with various concentrations (20, 40, and 60 µg/mL) of BAL-CK-GNPs and control (free medium) for an additional 24 h at 37 °C and 5% CO₂ in an incubator. Total RNA was extracted from the cells using 500 µL of TRIzol reagent (Invitrogen, CA, USA). First, 500 ng of total RNA was reverse transcribed using the AmfiRivert cDNA Synthesis Platinum Enzyme Mix (GenDEPOT). The reaction was performed using the CFX96™ real-time RT-PCR system with SYBR Premix ExTaq™ II (TaKaRa). The qRT-PCR was performed using 50 ng of cDNA in a 20 µL reaction

volume with AmfiSure qGreen Q-PCR Master Mix (GenDEPOT). qRT-PCR experiments were conducted in triplicate across three independent runs ($n=3$) to ensure accuracy and consistency. Target gene expression was quantified using the comparative Ct method ($\Delta\Delta C_t$), with relative expression levels presented as $2^{-\Delta\Delta C_t}$. The ratios of target genes to the housekeeping gene β -actin were compared across different groups for analysis. The apoptosis-related primers used in this study are listed in Table 1.

Transcriptomic analysis of BAL-CK-GNPs treated in AGS cells

The purity of the isolated RNA was assessed using a NanoDrop 1000 spectrophotometer (Thermo Fisher Scientific, Waltham, MA, USA) and an Agilent 2100 Bioanalyzer (Agilent Technologies, USA). The quality and integrity of the isolated RNA were evaluated. The isolated RNA samples were subjected to RNA sequencing. For RNA sequencing, libraries were prepared for the untreated control group and different concentrations of BAL-CK-GNPs-treated samples using the NovaSeq platform, following the manufacturer's protocol at DNA Link (Seoul, Republic of Korea). RNA-seq libraries were prepared to obtain the transcriptomic profiles of the samples. To identify the genes that were significantly differentially expressed between the control and treated samples, a clustering algorithm was applied to the overlapping genes. Hierarchical clustering was performed using Cluster v3.0 software (<https://www.encodeproject.org/software/cluster/>). An expression heatmap was generated using the Euclidean distance and average linkage methods, and MeV 4.9.0 software was used to construct the heatmap. A list of differentially expressed genes (DEGs) was used for further analysis. An online tool, ShinyGO bioinformatics (<https://david.ncifcrf.gov/>), was used to analyze the gene ontology (GO) and Kyoto Encyclopedia of Genes and Genomes (KEGG pathway). Further protein–protein interaction (PPI) network was identified using STRING, and these data were visualized in Cytoscape v3.8.1. KEGG pathway and GO analyses were performed on the selected DEGs (fold change ≥ 1). This analysis provides insights into the biological functions and pathways associated with the differentially expressed genes.

Statistical analysis

All data were expressed as the mean \pm standard deviation of three independent experiments. Statistical analysis was performed using the GraphPad Prism 8. The student's *t* test was performed to compare the treatment groups with the control group. * $p < 0.05$, ** $p < 0.01$, and *** $p < 0.001$ were considered statistically significant.

Table 1 List of primer sequences used in this study

| Gene | Forward primer (5'–3') | Reverse primer (5'–3') |
|----------------|-----------------------------|----------------------------|
| β -Actin | 5'-CGGGAAATCGTGCGTGAC-3' | 5'-AGCTCTTCTCCAGGGAGGA-3' |
| Bcl-2 | 5'-GTGGTGGAGGAAGCTTCTCAG-3' | 5'-GTTCCACAAAGGCATCCAG-3' |
| Bax | 5'-AGCAAAGTGGTCTCAAGGC-3' | 5'-CCACAAAGATGGTCACTGTC-3' |
| Cyt. C | 5'-GAGGCAAGCATAAGACTGG-3' | 5'-TACTCCATCAGGGTATCTC-3' |
| Cas. 9 | 5'-CGCCACCATCTTCTCCCTG-3' | 5'-GCCATGGTCTTCTGCTCA-3' |
| Cas. 3 | 5'-CCTCAGAGAGACATTCATG-3' | 5'-GCAGTAGTCGCTCTGAAG-3' |

Results

Characterization of BAL-CK-GNPs

Our previous study (Kim et al. 2024) provided a detailed analysis of the optimal conditions and characterization of BAL-CK-GNPs. The optimal synthesis parameters, which yielded the highest peaks, included bacterial growth at O.D. 1.0, a gold salt concentration of 2.0 mM, CK concentration of 0.3 mM, and a pH of 7. FTIR analysis confirmed the successful loading of CK onto the newly synthesized BAL-CK-GNPs, as evidenced by shifts in characteristic peaks corresponding to C=O stretching, C=C alkene, CH₂ bending, CH₃ bending, PO₂⁻ stretching, C-H alkene, P-O-C twisting, N-H bending, and C-H stretching (amide II). TEM imaging revealed spherical nanoparticles with sizes ranging from 10 to 25 nm, confirming their nanoscale dimensions. In addition, element mapping, SAED pattern, EDX spectrum, and zeta potential (mV) analysis further validated the successful synthesis and stability of BAL-CK-GNPs. A summary of these results is presented in Table 2, while a more detailed analysis can be found in our previously published study (Kim et al. 2024).

CK quantification in drug-loaded and released BAL-CK-GNPs

Accurate quantification of ginsenoside CK in drug-loaded and released BAL-CK-GNPs is essential for evaluating the efficiency of the nanoformulation. Given CK's high solubility in methanol, the majority of the released drug was expected to dissolve in the MeOH fraction (Kim et al. 2019). Supplementary Fig. 1A, B illustrates the measured CK concentrations in both the drug-loaded nanoparticles and the released fraction. The retention times (RT) were recorded at 3.46 and 3.47 min, with corresponding peak area responses of 17,969 and 29,938, peak heights of 9,005 and 14,358, and signal-to-noise ratios of 15,143.27 and 19,502.88, respectively. Supplementary Fig. 1C presents the standard CK

Table 2 Synthesis and characterization of BAL-CK-GNPs

| Properties | Value/shape | Peak assignment | |
|-----------------------|---|-----------------|------------|
| | | CK | BAL-CK-GNP |
| Physical | Bacterial biomass (OD600) | 1 | – |
| | GNP concentration (mM) | 2 | – |
| | CK concentration (mM) | 0.3 | – |
| | pH | 7 | – |
| FTIR | C=O stretch, C=C alkene | – | 1654.74 |
| | CH ₂ bend | – | 1453.57 |
| | CH ₃ bend | – | 1387.02 |
| | PO ₂ ⁻ stretching | – | 1076.79 |
| | C-H alkene | – | 646.85 |
| | P-O-C twisting | – | 1042.63 |
| | N-H bending and C-H stretching (amide II) | – | 1546.03 |
| TEM | Shape | Spherical | – |
| | Size (nm) | 10–25 | – |
| Element mapping (GNP) | Detect | – | – |
| SAED pattern | Detect | – | – |
| EDX spectrum | Detect | – | – |
| Zeta potential (mV) | –40.33 | – | – |

calibration curve, described by the equation $y = (1495 \times X) - 960.3$ ($R^2 = 99.98\%$), confirming a strong linear correlation. Supplementary Fig. 1D summarizes the drug release and loading data. Following sonication, approximately 16.664 $\mu\text{g/g}$ of CK was released into the medium. The drug loading efficiency of BAL-CK-GNPs was determined to be $\sim 1.67\%$, indicating the effectiveness of the formulation in encapsulating and releasing CK.

Cytotoxicity of BAL-CK-GNPs on various cancer cell lines

The cytotoxic potential of BAL-CK-GNPs was evaluated against multiple cancer cell lines, including A549, HT-29, and AGS, using the MTT assay. The concentrations of BAL-CK-GNPs used in this study ranged from 20 to 80 $\mu\text{g/mL}$. Results demonstrated a significant, dose-dependent reduction in cell viability across all tested cancer cell lines (Fig. 1). Specifically, BAL-CK-GNPs treatment resulted in an IC_{50} value of 43.72 $\mu\text{g/mL}$ in AGS cells (Fig. 1C), while IC_{50} values of 54.04 $\mu\text{g/mL}$ and 51.56 $\mu\text{g/mL}$ were observed in A549 and HT-29 cells, respectively (Fig. 1A, B). The observed dose-dependent cytotoxicity indicates the potential of BAL-CK-GNPs as an effective anti-cancer agent. In addition to quantitative cell viability measurements, morphological changes indicative of cell death was visually confirmed through optical microscopy of BAL-CK-GNPs on each cancer cell line (Fig. 1, right panels). Based on these results, AGS cells were selected for further investigation due to their higher sensitivity to BAL-CK-GNPs treatment.

Intracellular localization and uptake analysis of BAL-CK-GNPs in AGS cells

TEM analysis was performed to investigate the intracellular distribution and impact of BAL-CK-GNPs in AGS cells (Fig. 2A). In the untreated control cells, the TEM images revealed the presence of normal cytoplasmic organelles with intact nuclei and mitochondria (Fig. 2A, left panel). However, following a 3-h treatment with BAL-CK-GNPs at a concentration of 60 $\mu\text{g/mL}$, the localization of the nanoparticles within AGS cells was distinctly observed. The TEM images indicated that the BAL-CK-GNPs were primarily transported into the cytosol via endosomes and lysosomes. Furthermore, the BAL-CK-GNPs were detected within key cellular compartments, including the outer and inner mitochondrial membranes, the nucleus, and the endoplasmic reticulum, suggesting effective intracellular distribution.

To further assess the internalization and penetration of BAL-CK-GNPs, cellular uptake was evaluated using EDF microscopy. This technique leverages the principle of blocking central light and focusing the remaining external light as condensed rings towards the sample, enhancing the visualization of scattering elements. In the control group, no bright white spots were observed, indicating the absence of nanoparticles. In contrast, following the 3-h incubation period, aggregated bright white spots were clearly visible in the treated group (Fig. 2B, left panel), indicating successful internalization of BAL-CK-GNPs by AGS cells. The observed bright white aggregates suggested the intracellular incorporation of nanoparticles via membrane-reactive pathways, likely involving binding and subsequent cellular entry.

Detection of apoptotic cell death in AGS cells

The induction of apoptosis in AGS cells following BAL-CK-GNP treatment was assessed through fluorescence staining with Hoechst 33258 and propidium iodide (PI) dyes (Fig. 3). Morphological changes associated with apoptosis were clearly identified using both staining methods. In untreated control cells, Hoechst 33258 staining showed no fluorescence within the nuclei, indicating a lack of apoptotic activity (Fig. 3A). Conversely, AGS cells treated with increasing concentrations of BAL-CK-GNPs (20, 40, and 60 µg/mL) displayed prominent morphological features of apoptosis, such as cell rounding and increased fluorescence intensity. PI staining was employed to detect necrotic or dead cells, as PI is only taken up by cells with compromised membrane integrity. No PI fluorescence was observed in the control group, confirming the absence of necrosis. However, treatment with lower concentrations of BAL-CK-GNPs (20, 40, and 60 µg/mL) resulted in a noticeable increase

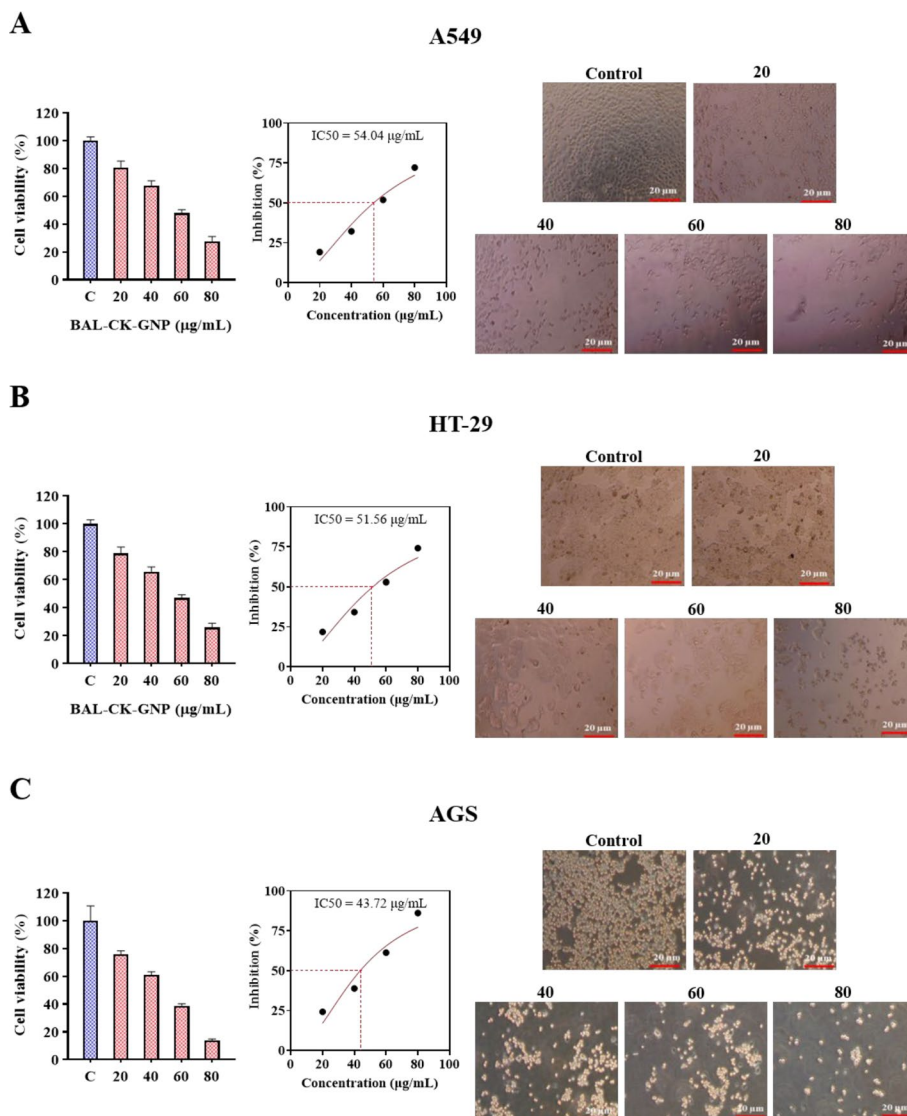


Fig. 1 Cytotoxicity activity of BAL-CK-GNPs against various cancer cells. **A** A549, **B** HT29, and **C** AGS were captured by light microscopy; it was performed in triplicate, and data were expressed as mean ± SE

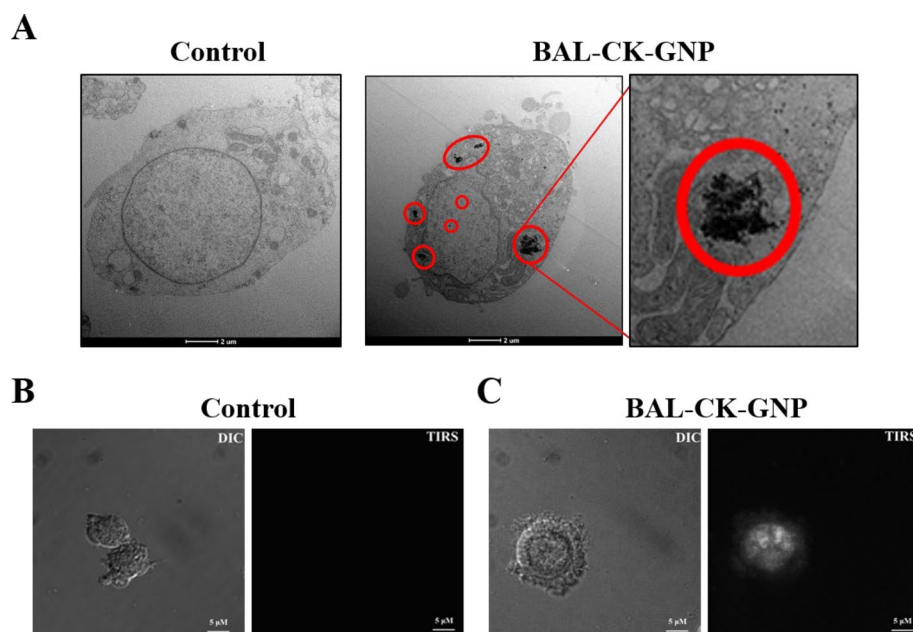


Fig. 2 **A** TEM images showing cellular uptake of BAL-CK-GNPs in AGS cells, with untreated cells on the left and treated cells on the right. **B, C** EDC microscopy images displaying BAL-CK-GNP detection: **B** DIC and TIRS images of untreated cells; **C** DIC and TIRS images of treated cells

in PI-positive cells, which appeared clustered in colonies (Fig. 3B). This increase in PI fluorescence, combined with Hoechst 33258 staining results, indicates that BAL-CK-GNPs induce both apoptosis and cell death in AGS cells. These findings strongly suggest that BAL-CK-GNPs exert a dose-dependent cytotoxic effect by triggering apoptotic pathways.

Mitochondrial alterations induced by BAL-CK-GNPs in AGS Cells

To evaluate mitochondrial changes in AGS cells, Mito-Tracker Green fluorescent dye staining was utilized, followed by analysis with a fluorescence microscope and EDF microscopy (Fig. 4). Fluorescence microscopy revealed significant morphological alterations in AGS cells treated with BAL-CK-GNPs compared to untreated controls, along with a marked increase in fluorescence intensity, indicating mitochondrial alterations (Fig. 4A). Further examination using EDF microscopy confirmed these findings. In the control group, the mitochondria maintained their normal structure within the cytoplasm, showing no visible changes. In contrast, AGS cells treated with BAL-CK-GNPs displayed clear damage to both the inner and outer mitochondrial membranes. This was evident from the aggregation of the dye into concentrated masses and distinct bright foci, indicative of mitochondrial disruption (Fig. 4B). These morphological differences between the treated and control groups highlight substantial mitochondrial damage caused by BAL-CK-GNPs exposure in AGS cells (Fig. 4).

Apoptotic pathway gene expression in AGS cells

The impact of BAL-CK-GNPs on the expression of key apoptotic pathway genes (Bax, Bcl-2, cytochrome C, and caspases 3 and 9) was evaluated in AGS cells (Fig. 5). The results revealed significant alterations in the mRNA expression levels of these genes following treatment. Specifically, the anti-apoptotic gene Bcl-2 was markedly downregulated, while the pro-apoptotic Bax gene showed a substantial upregulation (Fig. 5A, B). Moreover, the expression of cytochrome C in nuclear DNA exhibited a significant increase, indicating mitochondrial involvement in the apoptotic process (Fig. 5E). Correspondingly, the expression levels of caspase 3 and caspase 9 genes were also significantly elevated compared to the control (Fig. 5C, D). The concentration-dependent treatment of BAL-CK-GNPs clearly induced apoptosis, as evidenced by these gene expression changes. Notably, the Bcl-2 gene expression was approximately five times lower than in untreated cells, whereas Bax expression was twice as high in the BAL-CK-GNPs-treated cells. These findings underscore the role of BAL-CK-GNPs in triggering apoptotic mechanisms within AGS cells.

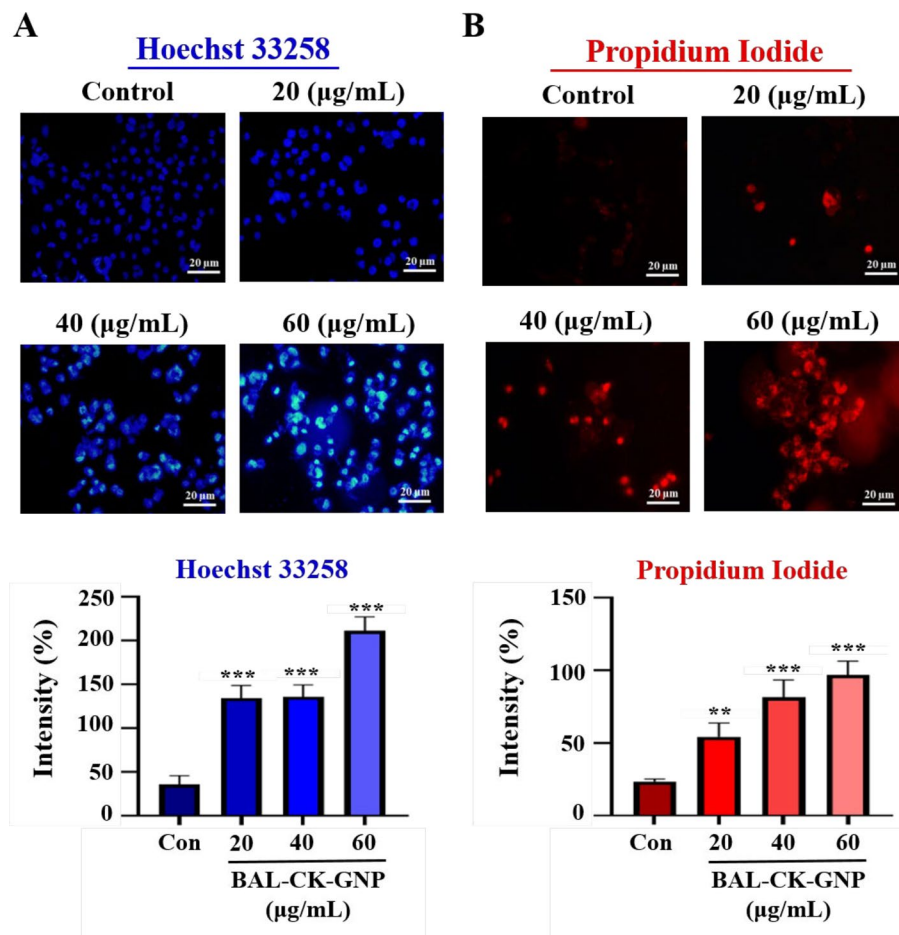


Fig. 3 Fluorescence microscopy analysis of apoptotic AGS cells treated with BAL-CK-GNPs at varying concentrations through the **A** Hoechst 33258 and **B** PI staining with a scale bar, of 20 µm

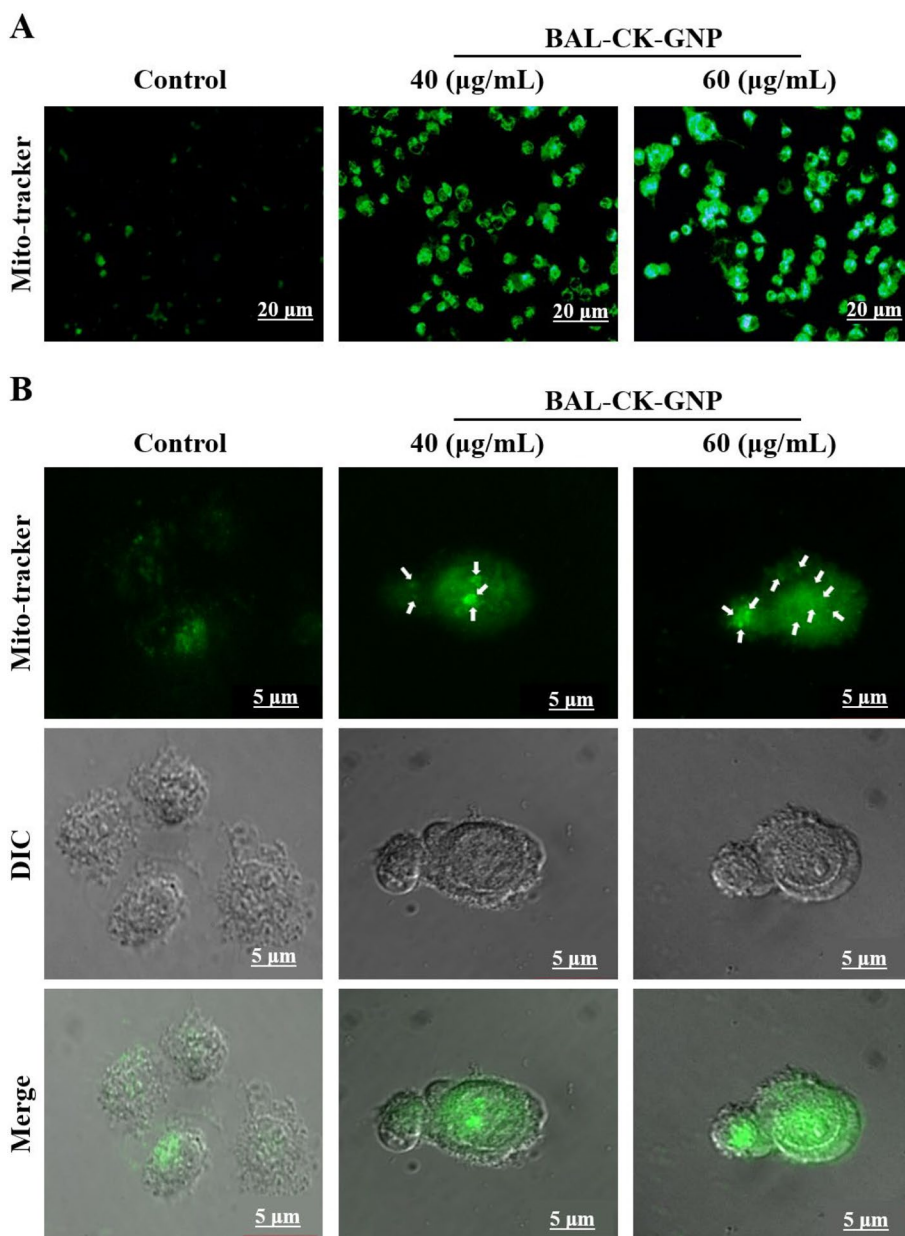


Fig. 4 Mitochondrial damage was assessed using fluorescence and EDF microscopy at various concentrations of BAL-CK-GNPs in AGS cells. **A** Mitotracker staining images obtained through fluorescence microscopy are displayed with a scale bar, of 20 μm. **B** Fluorescence microscopy images of Mitotracker staining are presented with a 5 μm scale bar and EDF microscopy images show moderate disorganization of the mitochondria

RNA sequencing: profiling DEGs and pathways in BAL-CK-GNPs-treated AGS cells

To explore the molecular mechanisms underlying BAL-CK-GNPs-induced cell death in AGS cells, RNA-seq transcriptome analysis was conducted (Fig. 6). The analysis aimed to identify changes in gene expression between the control group and the group treated with BAL-CK-GNPs. The differential gene expression patterns were visualized using volcano plots (Fig. 6A), revealing a total of 26,255 genes with altered expression

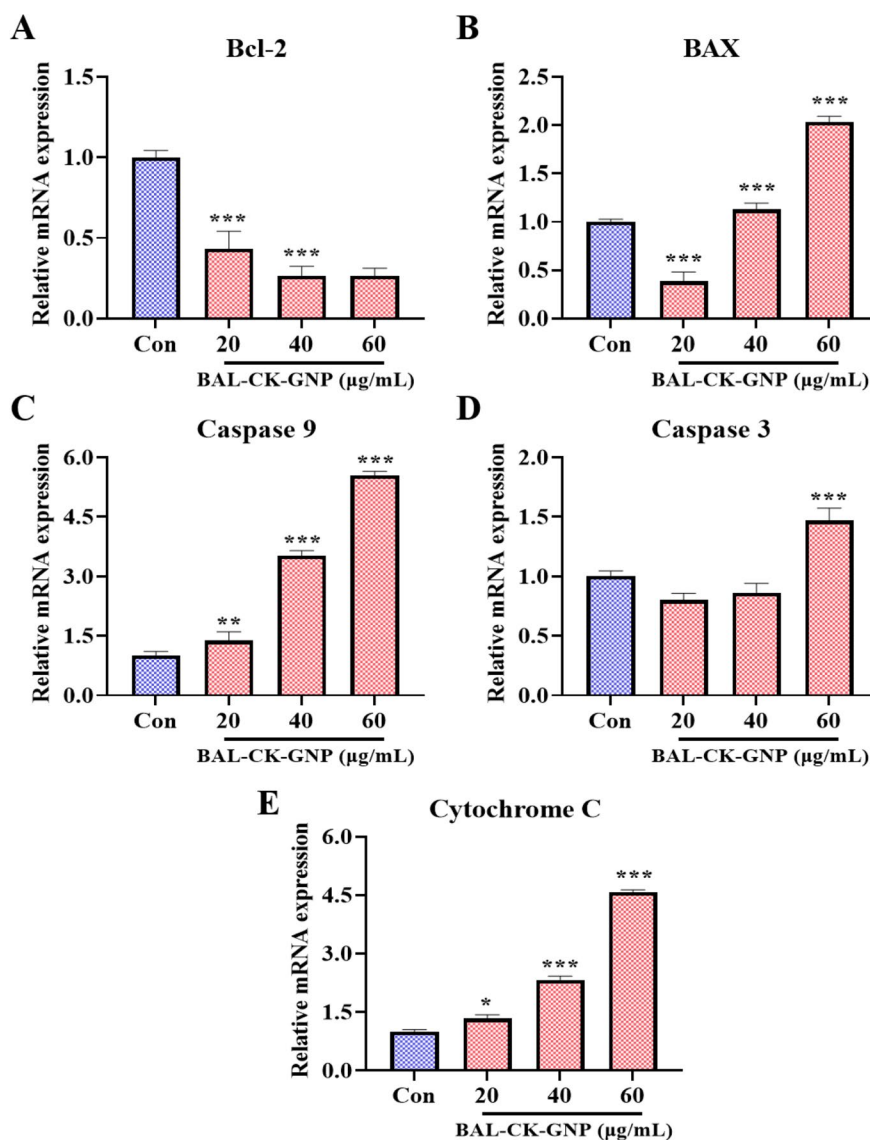


Fig. 5 Effect of BAL-CK-GNPs on apoptotic gene expression in AGS cells. The mRNA expression levels of **A** Bcl-2, **B** Bax, **C** Caspase 9, **D** Caspase 3, and **E** Cytochrome c

levels in the treated cells compared to the control (Supplementary Table 1). Out of these, 78 genes were upregulated, and 146 were downregulated, based on a threshold of $\log_2(\text{fold change}) \geq |1.0|$ and a p value of ≥ 0.05 (Fig. 6B and Supplementary Table 2).

To gain further insight into the biological significance of these DEGs, we performed the KEGG pathway and GO analysis using the ShinyGO databases. The 224 DEGs identified in the treated cells were subjected to KEGG and GO analyses to determine the key pathways affected by BAL-CK-GNPs. The results indicated that the treatment influenced several critical molecular signaling pathways related to cancer progression, such as ferroptosis, glutathione metabolism, necroptosis, and the NF- κ B, IL-17, and TNF signaling pathways, which were significantly enriched based on gene counts

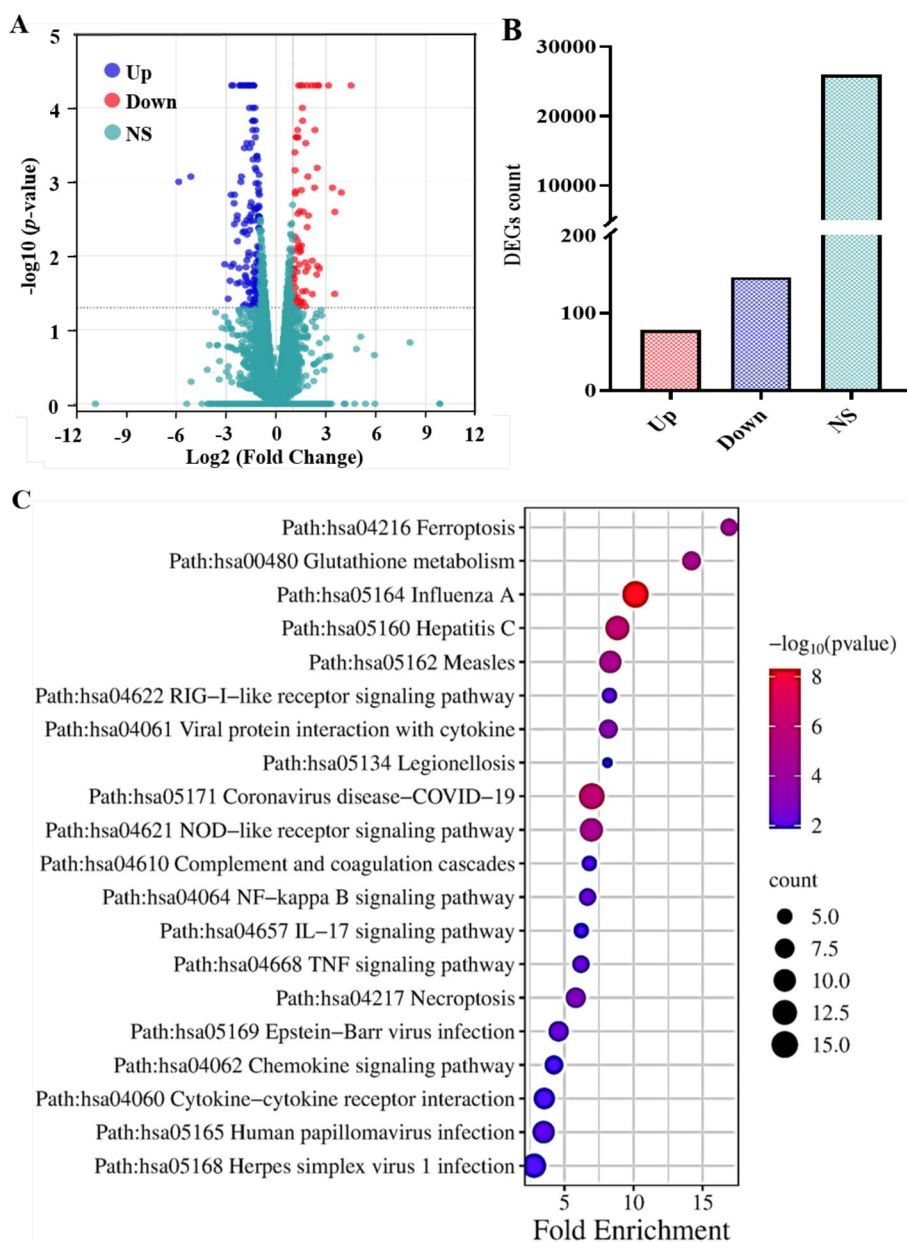


Fig. 6 **A** Volcano plot displaying the DEGs in AGS cells treated with BAL-CK-GNPs compared to untreated AGS cells. **B** Summary of the number of DEGs, indicating those that are upregulated, downregulated, and non-significant. **C** KEGG pathway

and p values (Fig. 6C and Supplementary Table 3). These findings suggest that BAL-CK-GNPs may exert anti-GC effects by modulating multiple key pathways involved in cell survival, inflammation, and PCD in AGS cells.

The GO analysis of the regulated genes revealed their involvement in key biological processes (BP), cellular components (CC), and molecular functions (MF) (Fig. 7). Within the BP category, treatment with BAL-CK-GNPs significantly influenced the regulation of the interferon (IFN) signaling pathway, as well as the production of IFN and IFN- β . In terms of CC, the analysis indicated the regulation of various cellular structures,

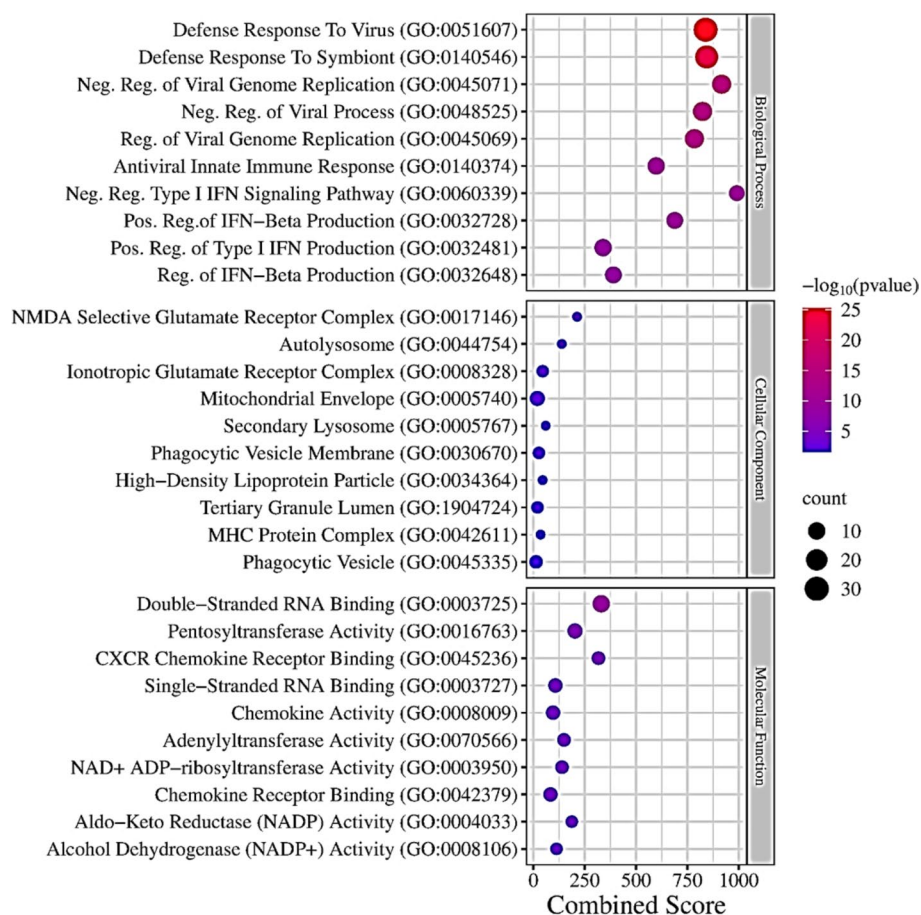


Fig. 7 Top significant GO terms for DEGs in BAL-CK-GNPs-treated cells primarily highlight pathways associated with cell death and inflammation

including mitochondria, autolysosomes, glutamate-related components, and phagocytic vesicles. In the MF category, BAL-CK-GNPs treatment notably affected RNA binding activity, pentosyltransferase functions, and chemokine regulation, among other molecular activities. The enrichment analysis indicated that the regulated genes were significantly associated with specific GO terms, as detailed in Supplementary Table 4. These findings provide insights into the specific gene functions and pathways modulated by BAL-CK-GNPs treatment.

Network analysis of DEGs in AGS cells treated with BAL-CK-GNPs

A comprehensive network analysis was conducted to examine the interactions of 146 proteins implicated in the regulation of cell death in AGS cells treated with BAL-CK-GNPs. Using NetworkAnalyst, a total of 621 interacting proteins were identified, expanding the network beyond the initial set of proteins (Supplementary Fig. 2). To highlight key interaction hubs, the top 20 proteins were ranked based on degree centrality and visualized with the cytoHubba plugin in Cytoscape (Fig. 8A and Supplementary Table 5). In addition, the top 20 interacting proteins were selected using alternative network metrics, including closeness, MCC, and EPC methods (Fig. 8B–D and Supplementary Table 5).

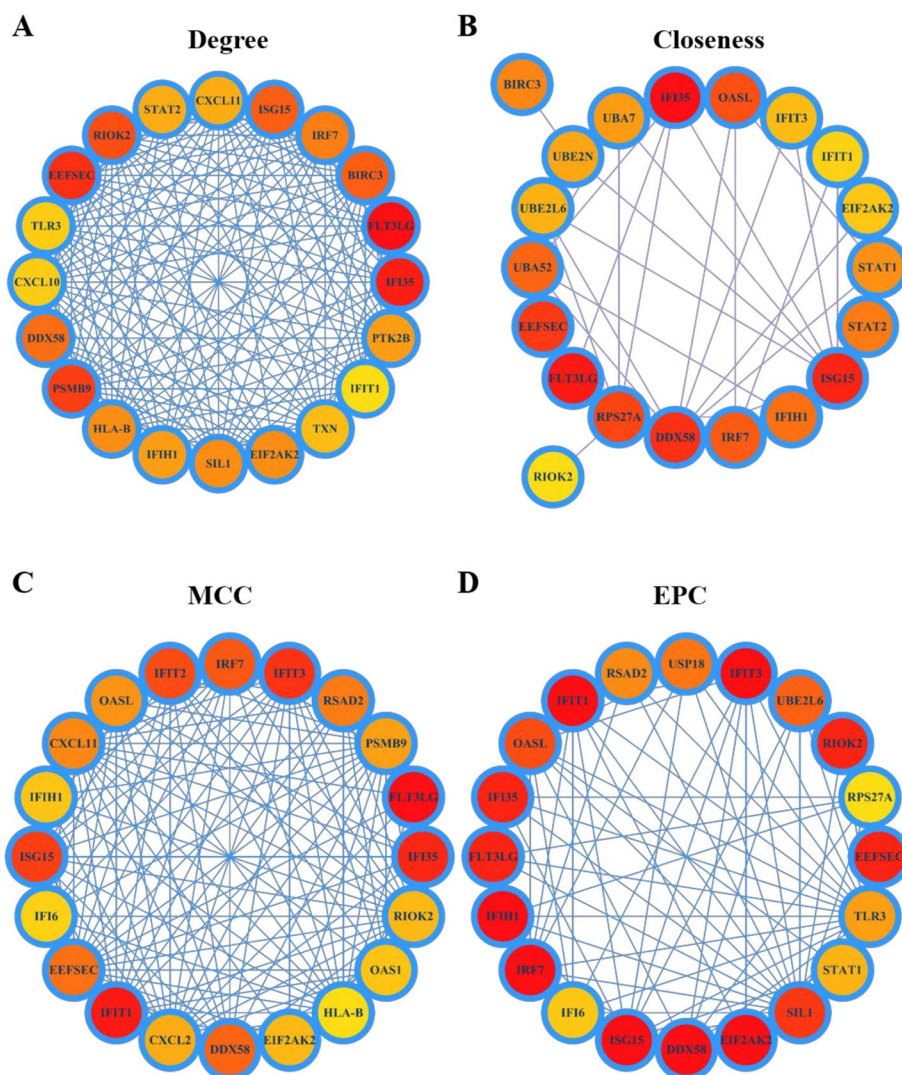


Fig. 8 PPI networks of significant DEGs were analyzed using four distinct methods: **A** degree centrality, **B** closeness centrality, **C** maximum clique centrality (MCC), and **D** edge percolated component (EPC). Each method identifies key interacting proteins, highlighting their roles in cellular processes

A Venn diagram was then constructed to identify overlapping proteins across these four ranking methods, pinpointing those most likely involved in regulating cell death. This analysis identified 10 common genes (IFI35, R1OK2, DDX58, IFIT1, ISG15, EIF2AK2, IFIH1, FLT3LG, EEFSEC, and IRF7) with significant interactions within the network (Fig. 9A, B). Among these, ISG15 emerged as the most highly connected protein, suggesting it may play a prominent role in mediating cell death following BAL-CK-GNPs treatment in AGS cells (Fig. 9B). These findings provide insight into potential protein targets for modulating cell death pathways in this cellular context.

Discussion

GNPs are widely applied in various medical fields, particularly in the targeted delivery and controlled release of therapeutic agents, including anticancer drugs, peptides, and antibodies (Oladipo et al. 2023). Numerous studies have demonstrated the potential

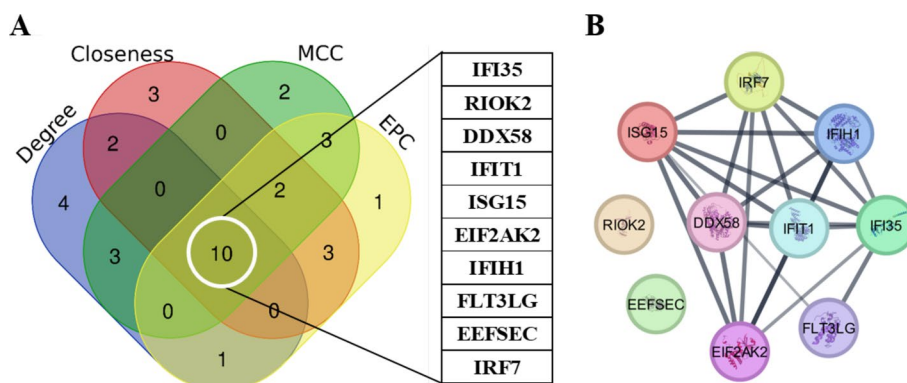


Fig. 9 **A** Venn diagram illustrating the overlap of proteins identified using four different methods of PPI analysis. **B** Interaction network of the 10 common proteins identified across these methods, highlighting their interconnectedness

of GNPs in enhancing drug delivery for cancer treatments, including agents, such as 5-fluorouracil, doxorubicin, and curcumin (Dhandapani et al. 2024). In addition, previous research has shown that CK and BAL-CK-GNPs exhibit anticancer and anti-inflammatory activities, respectively (Gwon et al. 2024; Kim et al. 2024; Tam et al. 2023). However, the specific effects of BAL-CK-GNPs in cancer studies remain unclear. Our findings demonstrate that BAL-CK-GNPs effectively induce anti-gastric cancer through PCD pathways and modulation of inflammation.

Recent studies have suggested that CK and microorganisms can be used for the biosynthesis of GNPs, which exhibit a color change from yellow to deep purple (Puja et al. 2022). In this study, BAL-CK-GNPs was displayed a similar purple hue, as detailed in (Kim et al. 2024). The BAL-CK-GNPs were characterized using FE-TEM, SAED, EDX, SEM, DLS, and XRD. A recent study by (Subhalakshmi et al. 2024) employed a similar experimental approach for nanoparticle characterization. Kim et al. (2019) was prepared DCY51T-AuCKNps through one-pot biosynthesis using *Lactobacillus kimchicus* DCY51T and CK, yielding results similar to our BAL-CK-GNPs (Y.-J. Kim et al. 2019).

GNPs can potentially improve CK stability over time, and conjugating *Gluconacetobacter liquefaciens* kh-1 and CK to GNP surfaces may further enhance both stability and nanoparticle internalization (Balusamy et al. 2023). This study examined the uptake and intracellular distribution of BAL-CK-GNPs in AGS cells through EDF and TEM techniques. Prior research highlighted that the success of anticancer therapies often depends on the efficient cellular internalization of therapeutic agents. Nanoparticle entry into cells is primarily driven by processes, such as macropinocytosis, clathrin-mediated endocytosis, and caveolae-mediated endocytosis (Zhang et al. 2017). For instance, studies have shown that doxorubicin-bound, responsive GNPs can improve intracellular drug delivery, thus overcoming multidrug resistance in cancer cells (Wang et al. 2011). This effect is largely due to efficient uptake via endocytosis and subsequent acid-triggered drug release inside cells (Zhang et al. 2022). In addition, results showed that BAL-CK-GNPs caused an increase in damaged nuclei, mitochondria, and cytoplasm. Prior studies suggest that morphological changes in these cellular structures often indicate cell death (Mi et al. 2022; Solovieva et al. 2022).

A comprehensive investigation of the impact of BAL-CK-GNPs on AGS cells involved a series of experimental analyses. These BAL-CK-GNPs demonstrated significant inhibition of cell proliferation activities at concentrations of 20, 40, 60, and 80 µg/mL. Apoptotic changes, evidenced by condensed nuclei and the presence of apoptotic bodies, were observed in BAL-CK-GNPs-treated cells compared to control cells with normal nuclei in Hoechst 33258 and PI staining. Moreover, treatment with DCY51T–AuCKNPs induced apoptotic alterations, characterized by the appearance of apoptotic nuclei in AGS and HT29 colon cancer cells (Y. J. Kim et al. 2019). Hence, the induction of apoptosis by BAL-CK-GNPs suggests a synergistic effect in AGS cells.

We also examined mitochondria, which play an important role in cell survival and energy delivery, cell fusion and division, and highly interconnected network functions (Rossmann et al. 2021). Treatment with BAL-CK-GNPs resulted in impairment of the mitochondrial outer membrane in AGS cells, as evidenced by dye accumulation and the formation of distinct foci within the mitochondria. Recently, CK-loaded GNPs synthesized from *Curtobacterium proimmune* K3 were considered promising agents for cancer treatment, as they facilitate intrinsic apoptosis by disrupting the mitochondrial outer membrane (Puja et al. 2022). Moreover, mitochondria are associated with modified *Bcl* family genes and *caspase-3* and *9*. *Bcl-2* and *BAX* are typical *Bcl*-related genes that play an important role in inhibiting and promoting apoptosis and cell death and regulating mitochondrial permeability and *cytochrome C* release. According to previous reports on the apoptotic mechanism, the role of mitochondrial cleavage was important (Ma & Yang 2016). *Bcl-2* is present in the nucleus, mitochondria, and endoplasmic reticulum and plays a pivotal role in stabilizing cell barrier function and inhibiting the action of apoptosis-related proteins. It is also known to regulate the dynamics of mitochondria and is involved in the regulation of fusion and cleavage of mitochondria (Lopez and Tait 2015). This suggests a protective effect on metabolic activity and regulation of insulin secretion. Thus, in this study, the *Bcl-2* gene showed 5 times lower expression levels than the control; the total *Bax/Bcl-2* ratio showed it was more than 4 times higher than control when BAL-CK-GNPs were treated long with increased expression of *Cyto C*, *Cas9*, and *Cas3* genes. In Hengartner et al., it has been reported that the expression of the *Bax* gene increases and the expression of the *Bcl-2* gene decreases simultaneously to promote apoptosis by binding to voltage-dependent anion channels (Hengartner and Horvitz 1994). Depolarization of mitochondrial membranes by BAL-CK-GNPs opens mitochondrial permeable transition pores and releases *cytochrome C* into the cytoplasm along with ATP in mitochondria. As a result, it promotes *caspase 9* and induces apoptosis by rearranging the CARD domain. Recent studies have highlighted the anti-oral cancer effects of beta-sitosterol, particularly through apoptosis marker analysis (Jayaraman et al. 2023b), and the mechanisms of calotropin in inhibiting cell growth and triggering apoptosis in HSC-3 cells (Jayaraman et al. 2023a). Similarly, our BAL-CK-GNPs exhibited strong anticancer activity, primarily by activating the intrinsic-mediated apoptosis pathway. This suggests a comparable apoptotic mechanism in our nanoparticle formulation.

Treatment with BAL-CK-GNPs resulted in 78 up-regulated and 146 down-regulated DEGs compared to control. KEGG pathway analysis identified ferroptosis, glutathione

metabolism, necroptosis, and anti-inflammatory (NF- κ B, IL-17, TNF, chemokines, and cytokines) pathways upon BAL-CK-GNPs treatment. Ferroptosis inhibits GC metastasis by modulating ROS and GSH levels (Tong et al. 2022). Dysregulation of GSH degradation enzymes like GGT can exacerbate oxidative stress in GC (Zhang et al. 2024). Similarly, necroptosis, another form of PCD, contributes to inflammation and tumor progression in GC (Li et al. 2023a, b). Inflammatory pathways modulate GC dynamics and are linked to GC cell survival and metastasis (Tong et al. 2022). The IL-17 and TNF pathways further amplify inflammation, promoting cancer cell proliferation and resistance to apoptosis (Li et al. 2023a, b). These interconnected pathways create a complex network that influences GC progression and metastasis.

Viral infections also play a role in cancer development, with several viruses linked to chronic inflammation, immune evasion, and genetic manipulation of host cells (MacLennan and Marra 2023; Ye et al. 2023). BAL-CK-GNPs treatment modulated viral pathways in AGS cells, with key modulation observed in pathways associated with influenza A, hepatitis C, measles, SARS-CoV-2, Epstein–Barr, human papillomavirus, and herpes simplex virus. These viral pathways are linked to GC progression through immune suppression and persistent inflammation, creating a pro-tumorigenic environment (Griffin 2021; Khan et al. 2023; Russell and Peng 2009; Thapa et al. 2024; Wei et al. 2024).

In addition, PPIs were analyzed, revealing 621 proteins interacting with key signaling pathways. The top 20 proteins were ranked, and eight proteins (IFI35, DDX58, IFIT1, ISG15, EIF2AK2, IFIH1, FLT3LG, and IRF7) were identified to regulate cell death and inflammatory pathways upon BAL-CK-GNPs treatment. These proteins have been associated with immune responses, tumor progression, and apoptosis regulation (Li et al. 2023a, b; Li et al. 2024a, b; Li et al. 2024a, b; Swaraj and Tripathi 2024). Our findings suggest that these proteins may play a crucial role in modulating GC through these pathways.

A major limitation of this study is the lack of validation of these genes at both mRNA and protein levels. In addition, BAL-CK-GNPs were only tested *in vitro*, requiring *in vivo* studies and clinical trials to confirm their therapeutic potential and safety. Future research should address these gaps for a comprehensive understanding.

Conclusion

In this study, BAL-CK-GNPs exhibited the highest inhibitory effect on cell proliferation in AGS cells compared to A549 and HT-29 cancer cell lines. Cellular uptake and penetration of BAL-CK-GNPs were confirmed, demonstrating their ability to damage cancer cells. Apoptosis induction and mitochondrial disruption further indicated the apoptotic effect on AGS cells, with the upregulation of apoptotic markers providing additional support for apoptosis induction. In addition, transcriptomic analysis suggested the involvement of BAL-CK-GNPs in activating ferroptosis, necroptosis, and pathways related to NF- κ B, TNF, and IL-17. PPI analysis identified eight proteins potentially regulating cell death and inflammation pathways. These findings provide initial evidence supporting the potential of BAL-CK-GNPs as anti-gastric cancer agents by shedding light on their mechanisms of action. Furthermore, for the extensive industrial application of BAL-CK-GNPs, it is imperative to conduct additional investigations, including *in vivo* studies and clinical trials.

Abbreviations

| | |
|------------------|---|
| GC | Gastric cancer |
| GNP | Gold nanoparticles |
| BAL | Bifidobacterium animalis subsp. lactis |
| CK | Compound K |
| DEGs | Differentially expressed genes |
| PCD | Programmed cell death |
| DAMP | Damage-associated molecular patterns |
| MRS | De Man, Rogosa, and Sharpe |
| MTT | 3-(4,5-Dimethyl-thiazol-2-yl)-2, 5-diphenyl tetrazolium bromide |
| NaCl | Sodium chloride |
| NaOH | Sodium hydroxide |
| FBS | Fetal bovine serum |
| IC ₅₀ | Inhibitory concentration |
| TEM | Transmission electron microscopy |
| EDF | Enhanced dark-field |
| qRT-PCR | Quantitative real time PCR |
| GO | Gene ontology |
| KEGG | Kyoto Encyclopedia of Genes and Genomes |
| PPI | Protein–protein interaction |
| PI | Propidium iodide |
| MCC | Maximum clique centrality |
| EPC | Edge percolated component |
| GSH | Glutathione |

Supplementary Information

The online version contains supplementary material available at <https://doi.org/10.1186/s12645-025-00310-9>.

Supplementary material 1: Fig. 1. Chromatographic analysis of CK in BAL-CK-GNP. Retention time of 3.46 and 3.47 minutes. Calibration curve for CK used for quantification, demonstrating a linear relationship between concentration and peak area. Table summarizing the analytical properties of CK. Fig. 2. PPI of the significant DEGs in AGS cells treated with BAL-CK-GNPs.

Supplementary material 2: Table 1. Total number of DEGs in AGS cells treated with BAL-CK-GNPs compared to untreated AGS cells.

Supplementary material 3: Table 2. Total significant number of DEGs in AGS cells treated with BAL-CK-GNPs compared to untreated AGS cells.

Supplementary material 4: Table 3. KEGG pathways of the total significant DEGs of BAL-CK-GNPs treated in AGS cells.

Supplementary material 5: Table 4. GO of the total significant DEGs of BAL-CK-GNPs treated in AGS cells.

Supplementary material 6: Table 5. PPI networks of significant DEGs were analyzed using four distinct methods: degree, closeness, MCC, and EPC.

Acknowledgements

Not applicable

Author contributions

A.S.: Methodology, Data analysis, Data curation, writing—Original Draft—Review & Editing; A.G.: Data analysis, writing—Original Draft; Y.J.K.: Conceptualization, Project administration, Supervision.

Funding

This work was supported by KDBIO Corp. and also supported by the fund "Cooperative Research Program for Agriculture Science and Technology Development (Project No. PJ01703502)" of the Rural Development Administration, Republic of Korea.

Availability of data and materials

No datasets were generated or analysed during the current study.

Declarations**Ethics approval and consent to participate**

Not applicable.

Consent for publication

Not applicable.

Competing interests

The authors declare no competing interests.

Received: 13 December 2024 Accepted: 10 February 2025

Published online: 02 April 2025

References

- Aguilar-Cazares D, Chavez-Dominguez R, Carlos-Reyes A, Lopez-Camarillo C, Hernandez de la Cruz ON, Lopez-Gonzalez JS (2019) Contribution of angiogenesis to inflammation and cancer. *Front Oncol*. <https://doi.org/10.3389/fonc.2019.01399>
- Balusamy SR, Perumalsamy H, Huq MA, Yoon TH, Mijakovic I, Thangavelu L, Yang DC, Rahimi S (2023) A comprehensive and systemic review of ginseng-based nanomaterials: synthesis, targeted delivery, and biomedical applications. *Med Res Rev* 43(5):1374–1410. <https://doi.org/10.1002/med.21953>
- Chehelgerdi M, Chehelgerdi M, Allela OQB, Pecho RDC, Jayasankar N, Rao DP, Thamaraianni T, Vasanthan M, Viktor P, Lakshmaia N, Saadh MJ, Amajd A, Abo-Zaid MA, Castillo-Acobo RY, Ismail AH, Amin AH, Akhavan-Sigari R (2023) Progressing nanotechnology to improve targeted cancer treatment: overcoming hurdles in its clinical implementation. *Mol Cancer* 22(1):169. <https://doi.org/10.1186/s12943-023-01865-0>
- Das S, Kundu M, Jena BC, Mandal M (2020) Chapter 25 - Causes of cancer: physical, chemical, biological carcinogens, and viruses. In: Kundu SC, Reis RL (eds) *Biomaterials for 3D tumor modeling*. Elsevier, Amsterdam, pp 607–641
- Dhandapani S, Xu X, Wang R, Puja AM, Kim H, Perumalsamy H, Balusamy SR, Kim Y-J (2021) Biosynthesis of gold nanoparticles using *Nigella sativa* and *Curtobacterium proimmune K3* and evaluation of their anticancer activity. *Mater Sci Eng C* 127:112214. <https://doi.org/10.1016/j.msec.2021.112214>
- Dhandapani S, Samad A, Liu Y, Wang R, Balusamy SR, Perumalsamy H, Kim Y-J (2024) Coprisin/Compound K conjugated gold nanoparticles induced cell death through apoptosis and ferroptosis pathway in adenocarcinoma gastric cells. *ACS Omega* 9(24):25932–25944. <https://doi.org/10.1021/acsomega.4c00554>
- Gong Y, Fan Z, Luo G, Yang C, Huang Q, Fan K, Cheng H, Jin K, Ni Q, Yu X, Liu C (2019) The role of necroptosis in cancer biology and therapy. *Mol Cancer* 18(1):100. <https://doi.org/10.1186/s12943-019-1029-8>
- Griffin DE (2021) Measles immunity and immunosuppression. *Curr Opin Virol* 46:9–14. <https://doi.org/10.1016/j.coviro.2020.08.002>
- Guan WL, He Y, Xu RH (2023) Gastric cancer treatment: recent progress and future perspectives. *J Hematol Oncol* 16(1):57. <https://doi.org/10.1186/s13045-023-01451-3>
- Gwon Y, Moon CY, Lee E-H, Im S-S, Kang H (2024) Anti-inflammatory effects of ginsenoside compound K in ethanol-stimulated macrophages by modulating sirtuin 1. *J Funct Foods* 117:106218. <https://doi.org/10.1016/j.jff.2024.106218>
- Hengartner MO, Horvitz HR (1994) *C. elegans* cell survival gene *ced-9* encodes a functional homolog of the mammalian proto-oncogene *bcl-2*. *Cell* 76(4):665–676. [https://doi.org/10.1016/0092-8674\(94\)90506-1](https://doi.org/10.1016/0092-8674(94)90506-1)
- Jayaraman S, Natarajan SR, Veeraraghavan VP, Jasmine S (2023a) Unveiling the anti-cancer mechanisms of calotropin: Insights into cell growth inhibition, cell cycle arrest, and metabolic regulation in human oral squamous carcinoma cells (HSC-3). *J Oral Biol Craniofac Res* 13(6):704–713. <https://doi.org/10.1016/j.jobcr.2023.09.002>
- Jayaraman S, Raj Natarajan S, Ponnusamy B, Veeraraghavan VP, Jasmine S (2023b) Unlocking the potential of beta sitosterol: Augmenting the suppression of oral cancer cells through extrinsic and intrinsic signalling mechanisms. *Saudi Dent J* 35(8):1007–1013. <https://doi.org/10.1016/j.sdentj.2023.08.003>
- Jin X, Tang J, Qiu X, Nie X, Ou S, Wu G, Zhang R, Zhu J (2024) Ferroptosis: emerging mechanisms, biological function, and therapeutic potential in cancer and inflammation. *Cell Death Discovery* 10(1):45. <https://doi.org/10.1038/s41420-024-01825-7>
- Khan S (2015) Potential role of *Escherichia coli* DNA mismatch repair proteins in colon cancer. *Crit Rev Oncol Hematol* 96(3):475–482. <https://doi.org/10.1016/j.critrevonc.2015.05.002>
- Khan S, Imran A, Khan AA, Abul Kalam M, Alshamsan A (2016) Systems biology approaches for the prediction of possible role of chlamydia pneumoniae proteins in the etiology of lung cancer. *PLoS ONE* 11(2):e0148530. <https://doi.org/10.1371/journal.pone.0148530>
- Khan S, Zaidi S, Alouffi AS, Hassan I, Imran A, Khan RA (2020) Computational proteome-wide study for the prediction of *Escherichia coli* protein targeting in host cell organelles and their implication in development of colon cancer. *ACS Omega* 5(13):7254–7261. <https://doi.org/10.1021/acsomega.9b04042>
- Khan I, Harshithkumar R, More A, Mukherjee A (2023) Human papilloma virus: an unraveled enigma of universal burden of malignancies. *Pathogens*. <https://doi.org/10.3390/pathogens12040564>
- Kim Y-J, Perumalsamy H, Markus J, Balusamy SR, Wang C, Ho Kang S, Lee S, Park SY, Kim S, Castro-Aceituno V, Kim SH, Yang DC (2019a) Development of *Lactobacillus kimchicus* DCY51T-mediated gold nanoparticles for delivery of ginsenoside compound K: in vitro photothermal effects and apoptosis detection in cancer cells. *Artif Cells Nanomed Biotechnol* 47(1):30–44. <https://doi.org/10.1080/21691401.2018.1541900>
- Kim S, Wang R, Dhandapani S, Kang K, Cho I-H, Kim Y-J (2024) Novel modified probiotic gold nanoparticles loaded with ginsenoside CK exerts an anti-inflammation effect via NF- κ B/MAPK signaling pathways. *Arab J Chem* 17(4):105650. <https://doi.org/10.1016/j.arabjc.2024.105650>
- Kumalasari MR, Alfanaar R, Andreani AS (2024) Gold nanoparticles (AuNPs): a versatile material for biosensor application. *Talanta Open* 9:100327. <https://doi.org/10.1016/j.talo.2024.100327>
- Lei Z-N, Teng Q-X, Tian Q, Chen W, Xie Y, Wu K, Zeng Q, Zeng L, Pan Y, Chen Z-S, He Y (2022) Signaling pathways and therapeutic interventions in gastric cancer. *Signal Transduct Target Ther* 7(1):358. <https://doi.org/10.1038/s41392-022-01190-w>
- Li M, Jiang P, Yang Y, Xiong L, Wei S, Wang J, Li C (2023a) The role of pyroptosis and gasdermin family in tumor progression and immune microenvironment. *Exp Hematol Oncol* 12(1):103. <https://doi.org/10.1186/s40164-023-00464-5>

- Li P, Zhou D, Chen D, Cheng Y, Chen Y, Lin Z, Zhang X, Huang Z, Cai J, Huang W, Lin Y, Ke H, Long J, Zou Y, Ye S, Lan P (2023b) Tumor-secreted IGF1 promotes proliferation and cytotoxic activity of CD8(+) T cells through PI3K/AKT/mTOR signaling pathway in colorectal cancer. *J Biomed Sci* 30(1):47. <https://doi.org/10.1186/s12929-023-00930-6>
- Li TH, Zhao BB, Qin C, Wang YY, Li ZR, Cao HT, Yang XY, Zhou XT, Wang WB (2024a) IFIT1 modulates the proliferation, migration and invasion of pancreatic cancer cells via Wnt/ β -catenin signaling. *Cell Oncol (Dordr)* 47(4):1253–1265. <https://doi.org/10.1007/s13402-024-00925-x>
- Li X, Ding N, Ma W, Zhang M (2024b) IFIH1-mediated post-transcriptional regulation of PTTG1 promotes proliferation and affects PHA-848125 sensitivity and prognosis in oropharyngeal carcinoma. *Am J Cancer Res* 14(5):2157–2171. <https://doi.org/10.62347/ylcq4222>
- Lopez J, Tait SWG (2015) Mitochondrial apoptosis: killing cancer using the enemy within. *Br J Cancer* 112(6):957–962. <https://doi.org/10.1038/bjc.2015.85>
- Ma DD, Yang WX (2016) Engineered nanoparticles induce cell apoptosis: potential for cancer therapy. *Oncotarget* 7(26):40882–40903. <https://doi.org/10.18632/oncotarget.8553>
- MacLennan SA, Marra MA (2023) Oncogenic viruses and the epigenome: how viruses hijack epigenetic mechanisms to drive cancer. *Int J Mol Sci*. <https://doi.org/10.3390/ijms24119543>
- Mary SJ, Veeravarmal V, Thankappan P, Arumugam P, Augustine PI, Franklin R (2024) Anti-cancer effects of green synthesized gold nanoparticles using leaf extract of *Annona muricata*. L against squamous cell carcinoma cell line 15 through apoptotic pathway. *Dent Res J* 21(1):14
- Mi X-J, Park H-R, Dhandapani S, Lee S, Kim Y-J (2022) Biologically synthesis of gold nanoparticles using *Cirsium japonicum* var *maackii* extract and the study of anti-cancer properties on AGS gastric cancer cells [Research Paper]. *Int J Biol Sci* 18(15):5809–5826. <https://doi.org/10.7150/ijbs.77734>
- Newton K, Strasser A, Kayagaki N, Dixit VM (2024) Cell death. *Cell* 187(2):235–256. <https://doi.org/10.1016/j.cell.2023.11.044>
- Oladipo AO, Lebelo SL, Msagati TAM (2023) Nanocarrier design-function relationship: the prodigious role of properties in regulating biocompatibility for drug delivery applications. *Chem Biol Interact* 377:110466. <https://doi.org/10.1016/j.cbi.2023.110466>
- Peng F, Liao M, Qin R, Zhu S, Peng C, Fu L, Chen Y, Han B (2022) Regulated cell death (RCD) in cancer: key pathways and targeted therapies. *Signal Transduct Target Ther* 7(1):286. <https://doi.org/10.1038/s41392-022-01110-y>
- Pistritto G, Trisciuglio D, Ceci C, Garufi A, D'Orazi G (2016) Apoptosis as anticancer mechanism: function and dysfunction of its modulators and targeted therapeutic strategies. *Aging* 8(4):603–619. <https://doi.org/10.18632/aging.100934>
- Puja AM, Xu X, Wang R, Kim H, Kim Y-J (2022) Ginsenoside compound K-loaded gold nanoparticles synthesized from *Curtobacterium proimmune K3* exerts anti-gastric cancer effect via promoting PI3K/Akt-mediated apoptosis. *Cancer Nanotechnol* 13(1):27. <https://doi.org/10.1186/s12645-022-00133-y>
- Rossmann MP, Dubois SM, Agarwal S, Zon LI (2021) Mitochondrial function in development and disease. *Dis Model Mech*. <https://doi.org/10.1242/dmm.048912>
- Russell SJ, Peng KW (2009) Measles virus for cancer therapy. *Curr Top Microbiol Immunol* 330:213–241. https://doi.org/10.1007/978-3-540-70617-5_11
- Sakore P, Bhattacharya S, Belemkar S, Prajapati BG, Elossaily GM (2024) The theranostic potential of green nanotechnology-enabled gold nanoparticles in cancer: A paradigm shift on diagnosis and treatment approaches. *Results Chem* 7:101264. <https://doi.org/10.1016/j.rechem.2023.101264>
- Santhosh PB, Genova J, Chamati H (2022) Green synthesis of gold nanoparticles: an eco-friendly approach. *Chemistry* 4(2):345–369. <https://doi.org/10.3390/chemistry4020026>
- Santos JP, Figueiredo J, Machado JC (2024) Gastric cancer genetics and its implications for diagnosis, prognosis, and treatment of the disease. *Korean J Helicobacter Upper Gastrointest Res* 24(2):103–112. <https://doi.org/10.7704/kjhugr.2024.0018>
- Solovieva M, Shatalin Y, Odinokova I, Krestinina O, Baburina Y, Mishukov A, Lomovskaya Y, Pavlik L, Mikheeva I, Holmuhamedov E, Akatov V (2022) Disulfiram oxy-derivatives induce entosis or paraptosis-like death in breast cancer MCF-7 cells depending on the duration of treatment. *Biochim Biophys Acta Gen Subj* 1866(9):130184. <https://doi.org/10.1016/j.bbagen.2022.130184>
- Sprooten J, De Wijngaert P, Vanmeerbeek I, Martin S, Vangheluwe P, Schlenner S, Krysko DV, Parys JB, Bultynck G, Vandenameele P, Garg AD (2020) Necroptosis in immuno-oncology and cancer immunotherapy. *Cells* 9(8):1823
- Subhalakshmi K, Veeraraghavan VP, Sivagnanam A, Thangasamy B, Francis AP (2024) Glucose-capped fisetin silver nanoparticles induced cytotoxicity and ferroptosis in breast cancer cells: a molecular perspective. *Inorg Chem Commun* 169:113004. <https://doi.org/10.1016/j.inoche.2024.113004>
- Swaraj S, Tripathi S (2024) Interference without interferon: interferon-independent induction of interferon-stimulated genes and its role in cellular innate immunity. *Mbio* 15(10):e02582–e2524. <https://doi.org/10.1128/mbio.02582-24>
- Tam DNH, Nam NH, Cuong NTK, Hung DT, Soa DT, Altom A, Tran L, Elhadad H, Huy NT (2023) Compound K: a systematic review of its anticancer properties and probable mechanisms. *Fundam Clin Pharmacol* 37(4):684–712. <https://doi.org/10.1111/fcp.12874>
- Thapa R, Magar AT, Shrestha J, Panth N, Idrees S, Sadaf T, Bashyal S, Elwakil BH, Sugandhi VV, Rojekar S, Nikhate R, Gupta G, Singh SK, Dua K, Hansbro PM, Paudel KR (2024) Influence of gut and lung dysbiosis on lung cancer progression and their modulation as promising therapeutic targets: a comprehensive review. *MedComm* 5(12):e70018. <https://doi.org/10.1002/mco2.70018>
- Tong X, Tang R, Xiao M, Xu J, Wang W, Zhang B, Liu J, Yu X, Shi S (2022) Targeting cell death pathways for cancer therapy: recent developments in necroptosis, pyroptosis, ferroptosis, and cuproptosis research. *J Hematol Oncol* 15(1):174. <https://doi.org/10.1186/s13045-022-01392-3>
- Tran KB, Lang JJ, Compton K, Xu R, Acheson AR, Henrikson HJ, Kocarnik JM, Penberthy L, Aali A, Abbas Q, Abbasi B, Abbasi-Kangevari M, Abbasi-Kangevari Z, Abbastabar H, Abdelmasset M, Abd-ElSalam S, Abdelwahab AA, Abdoli G, Abdulkadir HA, Murray CJL (2022) The global burden of cancer attributable to risk factors, 2010–19: a systematic analysis for the Global Burden of Disease Study 2019. *Lancet* 400(10352):563–591. [https://doi.org/10.1016/S0140-6736\(22\)01438-6](https://doi.org/10.1016/S0140-6736(22)01438-6)

- Wang F, Wang YC, Dou S, Xiong MH, Sun TM, Wang J (2011) Doxorubicin-tethered responsive gold nanoparticles facilitate intracellular drug delivery for overcoming multidrug resistance in cancer cells. *ACS Nano* 5(5):3679–3692. <https://doi.org/10.1021/nn200007z>
- Wang Y, Imran A, Shami A, Chaudhary AA, Khan S (2021) Decipher the helicobacter pylori protein targeting in the nucleus of host cell and their implications in gallbladder cancer: an insilico approach. *J Cancer* 12(23):7214–7222. <https://doi.org/10.7150/jca.63517>
- Wang S, He H, Qu L, Shen Q, Dai Y (2024) Dual roles of inflammatory programmed cell death in cancer: insights into pyroptosis and necroptosis. *Front Pharmacol* 15:1446486. <https://doi.org/10.3389/fphar.2024.1446486>
- Wei M, Li Q, Li S, Wang D, Wang Y (2024) Multifaceted roles of cGAS-STING pathway in the lung cancer: from mechanisms to translation. *PeerJ* 12:e18559. <https://doi.org/10.7717/peerj.18559>
- Wessler S, Krisch LM, Elmer DP, Aberger F (2017) From inflammation to gastric cancer – the importance of Hedgehog/GLI signaling in Helicobacter pylori-induced chronic inflammatory and neoplastic diseases. *Cell Commun Signal* 15(1):15. <https://doi.org/10.1186/s12964-017-0171-4>
- Ye R, Wang A, Bu B, Luo P, Deng W, Zhang X, Yin S (2023) Viral oncogenes, viruses, and cancer: a third-generation sequencing perspective on viral integration into the human genome. *Front Oncol* 13:1333812. <https://doi.org/10.3389/fonc.2023.1333812>
- Zhang J, Li J, Shi Z, Yang Y, Xie X, Lee SM, Wang Y, Leong KW, Chen M (2017) pH-sensitive polymeric nanoparticles for co-delivery of doxorubicin and curcumin to treat cancer via enhanced pro-apoptotic and anti-angiogenic activities. *Acta Biomater* 58:349–364. <https://doi.org/10.1016/j.actbio.2017.04.029>
- Zhang J, Lin W, Yang L, Zhang A, Zhang Y, Liu J, Liu J (2022) Injectable and pH-responsive self-assembled peptide hydrogel for promoted tumor cell uptake and enhanced cancer chemotherapy. *Biomater Sci* 10(3):854–862. <https://doi.org/10.1039/d1bm01788h>
- Zhang T, Yao C, Zhou X, Liu S, Qi L, Zhu S, Zhao C, Hu D, Shen W (2024) Glutathione-degrading enzymes in the complex landscape of tumors (Review). *Int J Oncol* 65(1):72. <https://doi.org/10.3892/ijo.2024.5660>

Publisher's Note

Springer Nature remains neutral with regard to jurisdictional claims in published maps and institutional affiliations.